Sensor Corrections for Sea-Bird SBE-41CP and SBE-41 CTDs*

Gregory C. Johnson

NOAA/Pacific Marine Environmental Laboratory, Seattle, Washington

John M. Toole

Physical Oceanography Department, Woods Hole Oceanographic Institution, Woods Hole, Massachusetts

Nordeen G. Larson

Sea-Bird Electronics, Inc., Bellevue, Washington

ABSTRACT

Sensor response corrections for two models of Sea-Bird Electronics, Inc., conductivity–temperature–depth (CTD) instruments (the SBE-41CP and SBE-41) designed for low-energy profiling applications were estimated and applied to oceanographic data. Three SBE-41CP CTDs mounted on prototype ice-tethered profilers deployed in the Arctic Ocean sampled diffusive thermohaline staircases and telemetered data to shore at their full 1-Hz resolution. Estimations of and corrections for finite thermistor time response, time shifts between when a parcel of water was sampled by the thermistor and when it was sampled by the conductivity cell, and the errors in salinity induced by the thermal inertia of the conductivity cell are developed with these data. In addition, thousands of profiles from Argo profiling floats equipped with SBE-41 CTDs were screened to select examples where thermally well-mixed surface layers overlaid strong thermoclines for which standard processing often yields spuriously fresh salinity estimates. Hundreds of profiles so identified are used to estimate and correct for the conductivity cell thermal mass error in SBE-41 CTDs.

1. Introduction

Salinity, temperature, and pressure are three basic-state variables that allow for the computation of ocean density and the associated physical properties of seawater. Temperature and pressure are generally measured directly, but salinity is usually calculated from these two variables together with conductivity. Such is the case with data acquired with a conductivity–temperature–depth (CTD) instrument, one of the observational mainstays of oceanography today. In many Sea-Bird Electronics, Inc. (SBE) CTDs, the temperature and conductivity sensors are arranged in a mechanically aspirated duct (Fig. 1). Temperature is measured with a pressure-protected, fast-response thermistor mounted near the duct intake, while conductivity is sensed inside a long, narrow, three-electrode cell located downstream of the intake. Accurate salinity data requires corrections for temporal and spatial mismatches in these sensor responses (Fofonoff et al. 1974; Gregg and Hess 1985; Lueck 1990; Lueck and Picklo 1990; Morison et al. 1994).

Given a known uniform flow rate in the ducted system, the time lag t_P, owing to the physical separation of the thermistor and the conductivity cell, can be estimated. Themistors used in CTDs generally have a short (<1 s) time response τ_T related to their thermal mass and boundary layer physics. Their responses are often modeled with single or multipole filters. Likewise, conductivity cells used in CTDs have a short response behavior that may be characterized by a time scale τ_C related to the cell flushing rate. Their response is often modeled with boxcar (or more complicated) convolu-

Corresponding author address: Dr. Gregory C. Johnson, NOAA/Pacific Marine Environmental Laboratory, 7600 Sand Point Way NE, Bldg. 3, Seattle, WA 98115.
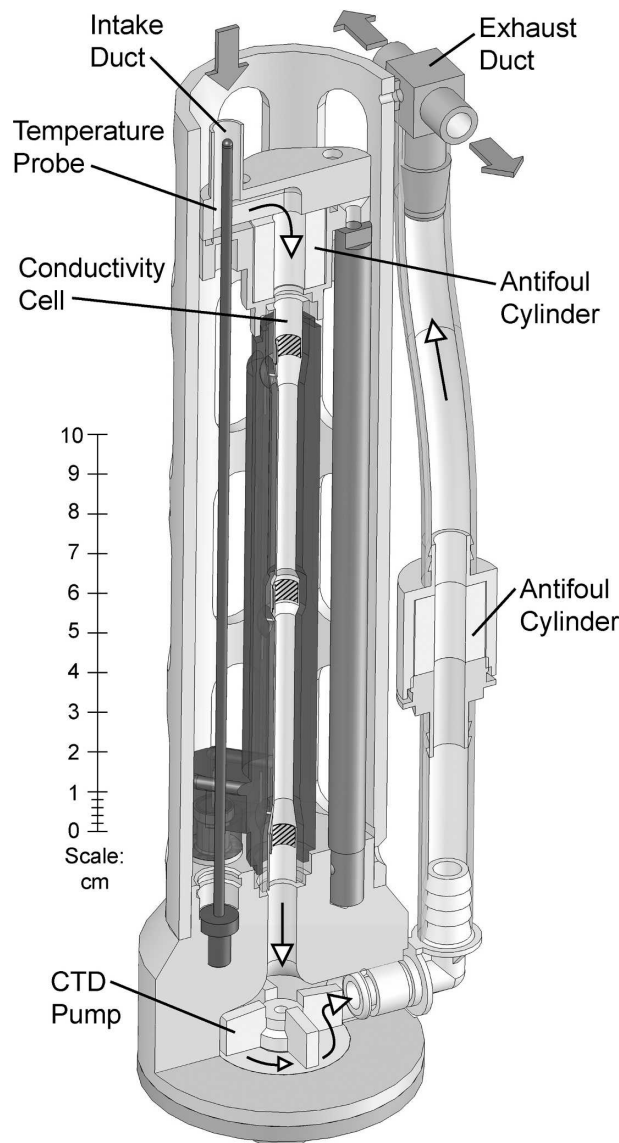E-mail: gregory.c.johnson@noaa.gov

FIG. 1. A cutaway, perspective, scaled rendering of the Sea-Bird Electronics, Inc., model SBE-41 and SBE-41CP CTD instruments. The two models are physically similar, but have different pumping and sampling strategies.

tion filters. In addition, SBE (and other) conductivity cells have a longer (order of 10 s) time-scale response related to the cell thermal mass and boundary layer physics, τ_{CTM} (Lueck 1990). Error deriving from the latter is easily detected in at least two situations. The first are cases when the CTD passes from a region of strong thermal gradient directly into a well mixed layer. Salinity, derived from the raw temperature and conductivity, will exhibit a "spike" that asymptotes to a uniform value as the cell temperature equilibrates with that of the layer (Lueck and Picklo 1990). The second are cases when a CTD is lowered through a strong ther-

mal gradient and is then raised back up. Again, due to cell thermal inertia, the potential temperature salinity (θ–S) curves will not overlay (e.g., Morison et al. 1994).

Following Lueck (1990), Lueck and Picklo (1990), and Morison et al. (1994), in a situation when a CTD passes through a 1°C step change in temperature at time $t = 0$, the temperature difference T_{diff} between the fluid within the conductivity cell and the water surrounding the thermistor can be approximately modeled as

$$T_{\mathrm{diff}}(t) = \alpha H(t) \exp[-(t - t_P)/\tau_{\mathrm{CTM}}], \qquad (1)$$

where α is the empirically determined magnitude of the temperature difference and $H(t)$ is the Heaviside step function [$H(t) = 0$ for $t < 0$ and $H(t) = 1$ for $t \geq 0$]. The temperature difference has initial magnitude α, but it decays exponentially with the time scale τ_{CTM}. More generally, the temperature difference is proportional to the temporal temperature gradient multiplied by $\alpha \times \tau_{\mathrm{CTM}}$. This fact can be appreciated by replacing $H(t)$ with a constant dT/dt in (1), and then integrating the result with respect to time. The model parameters α and τ_{CTM} depend mostly on the flow rate through the cell and the physical properties of the cell and its protective (partially insulating) jacket. As cell flow rate is increased, α, τ_{CTM}, and hence T_{diff}, are all reduced.

To our knowledge, detailed sensor response corrections have not been previously quantified for unmodified SBE-41 and SBE-41CP CTDs. These CTDs are used for energy-limited autonomous profiling applications and widely employed on Argo profiling floats (Roemmich et al. 2004). Here we develop response correction procedures for these two instruments. The operations of these instruments are discussed in section 2 with reference to the more familiar CTD model SBE-9. Then the datasets used for the present analyses are described in section 3. In sections 4 and 5, respectively, sensor responses and their corrections for SBE-41CP and SBE-41 data are investigated. The results are summarized in section 6, other considerations when correcting CTD sensor responses are outlined, and possible courses of action for improving the error correction are discussed.

2. SBE-41CP and SBE-41 CTDs

Argo is currently installing a near-global array of profiling floats to measure the temperature and salinity of the upper 2 km of the ocean (presently excluding areas with seasonal ice cover and the continental shelves). Companion efforts to autonomously sample the ice-covered oceans are being developed (e.g., E. Fahrbach, O. Bobelg and O. Klatt 2005, personal communication; Krishfield et al. 2006). These pro-

grams have a salinity accuracy goal of ± 0.01 PSS-78, which warrants correction of the sensor response errors outlined above. SBE builds two slightly different CTDs for such applications, the SBE-41 and the SBE-41CP (Fig. 1). Both have physical configurations and sensors similar to the long-used and well-studied SBE-9. There are, however, several differences among the SBE-41, SBE-41CP, and SBE-9. The first two have polyurethane jackets around the conductivity cell instead of the epoxy jacket used for the SBE-9. These materials have different densities, heat capacities, and thermal conductivities, all of which factor into the conductivity cell thermal mass error (Lueck 1990). In addition, the vertical velocities of the autonomous profilers on which the SBE-41 and SBE-41CP are deployed are often much less than that of the SBE-9 when deployed with a shipboard winch. Slower vertical velocity may reduce heat exchange between the cell and the exterior ambient fluid, increasing the size of the cell thermal mass error. On the other hand, these slower velocities lessen error size by reducing the temporal temperature gradients seen by the instruments. Finally, the SBE-41 and SBE-41CP employ different pumping and sampling strategies to balance the desire to reduce sensor response errors against the need to minimize energy consumption, as discussed below. Neither the SBE-41 nor the SBE-41CP currently makes internal corrections for the sensor responses discussed herein.

An SBE-9 with standard configuration has a continuous pumping rate of about 0.025 L s^{-1} (which, with an inside diameter of 4 mm for the conductivity cell, results in a mean velocity $V = 2.0$ m s^{-1} through the conductivity cell) and a 24-Hz sampling rate. The SBE-41CP (continuous profiling) in standard configuration has a pumping rate of 0.011 L s^{-1} ($V = 0.85$ m s^{-1}) and can record 0.7-s averages of conductivity, temperature, and pressure at rates as frequent as 1 Hz. The extensive SBE-41CP data acquired during a profile can be bin averaged or decimated internally to reduce size before telemetry if desired. In contrast, the SBE-41 CTD is designed as a spot-sampling instrument. When a CTD sample is required, the SBE-41 pump turns on to produce a flow rate of 0.034 L s^{-1} ($V = 2.7$ m s^{-1}) for a 2.5-s interval; temperature, pressure, and conductivity are measured during the last second of that interval. Though not actively pumped between samples, the duct system of the SBE-41 may still ventilate if the intake is oriented into an ambient flow (such as that experienced during float ascent). This orientation places the exhaust ducts perpendicular to the flow, inducing a pressure differential in the system. Laboratory experiments suggest that the ventilation rate increases linearly with increasing differential pressure up to 100 Pa, with a flow

rate of 2.4×10^{-5} L s^{-1} for a 1-Pa head. The ascent rate is not well known for Webb Research Corporation Autonomous Profiling Explorer (APEX) floats that employ Service Argos telemetry. However, engineering data (D. Swift 2005, personal communication) from new APEX Iridium/GPS floats with the same ascent algorithms as the older APEX Argos floats has shown that the ascent rate can vary between 0.06 and 0.12 dbar s^{-1} during a profile; the mean ascent rate ($\pm$standard deviation) is 0.09 (± 0.03) dbar s^{-1}. These results, coupled with simple Bernoulli calculations, suggest that the induced flow within a SBE-41 aboard a typical APEX float is about 0.008 m s^{-1}.

Rough estimates of some sensor response correction time scales may be obtained from simple empirical formulas developed and used at SBE that are a function of pump rate, Q (expressed in L s^{-1}). For the thermistor time scale, $\tau_T \sim 0.500$ s $+ Q^{-1}(2.86 \times 10^{-4}$ L), which yields 0.53 s for the SBE-41CP and 0.51 s for the SBE-41, with estimated errors of about $\pm 10\%$. For the short conductivity cell time scale, $\tau_C \sim Q^{-1}(1.80 \times 10^{-4}$ L), which yields 0.17 s for the SBE-41CP and 0.05 s for the SBE-41, with estimated errors of $\pm 15\%$. For the physical separation transit time, $t_P \sim Q^{-1}(2.13 \times 10^{-4}$ L), which yields 0.20 s for the SBE-41CP and 0.06 for the SBE-41, with estimated errors of about $\pm 5\%$. Morison et al. (1994) developed empirical formulas for the conductivity cell thermal mass error model parameters of the SBE-9: $\alpha = 0.0264$ V$^{-1} + 0.0135$ and $\tau_{\mathrm{CTM}} = 2.7858$ V$^{-1/2} + 7.1499$ s. For the nominal SBE-9 pump rate, these yield $\tau_{\mathrm{CTM}} = 9.1$ s, $\alpha = 0.027$, and $\alpha \times \tau_{\mathrm{CTM}} = 0.24$ s. Straightforward application of these formulas to the SBE-41CP gives $\tau_{\mathrm{CTM}} = 10.2$ s, $\alpha = 0.046$, and $\alpha \times \tau_{\mathrm{CTM}} = 0.45$ s. Similarly for the SBE-41 during pumping they give $\tau_{\mathrm{CTM}} = 8.8$ s, $\alpha = 0.023$, and $\alpha \times \tau_{\mathrm{CTM}} = 0.21$ s; for times when the pump is off they give $\tau_{\mathrm{CTM}} \sim 38$ s, $\alpha \sim 3.3$, and $\alpha \times \tau_{\mathrm{CTM}} \sim 127$ s. However, direct application of the SBE-9 α and τ_{CTM} formulas to the SBE-41 and SBE-41CP is questionable given differences in pump rates, cell jacketing materials, and profiling speeds (Morison et al. 1994). Moreover, given that the ventilation rate for the SBE-41 with the pump off is an estimate, the uncertainties for these last numbers are even larger than for the others.

The above estimates suggest that the SBE-41CP conductivity cell thermal mass error may be twice that of the SBE-9. Since the SBE-9 samples at 24 Hz, much faster than τ_{CTM}, the time history of temperature change is well measured, so a simple correction for the effects of conductivity cell thermal inertia on the salinity estimates can be applied (Lueck 1990; Lueck and Picklo 1990; Morison et al. 1994). For the SBE-41CP, continuous pumping means that the conductivity cell

thermal inertia should also be relatively easy to model, and the 1-Hz sampling rate, still shorter than the expected τ_{CTM}, means that the temperature time history should be reasonably well resolved. The intermittent pumping and sampling strategy of the SBE-41 complicates the modeling of the sensor response errors in at least three ways. First, there are two very different sets of conductivity cell thermal mass response model coefficients depending on pump state. Given the short duration of the 2.5-s pumping time with respect to either the pumped or unpumped value of τ_{CTM}, it seems likely that the effective τ_{CTM} will be larger than the pumped estimate. However, the effective α during sampling is likely to be closer to the smaller, pumped estimate. Second, because of the sparse and intermittent sampling, the temporal temperature and conductivity gradients are not sampled well with respect to τ_{CTM}, let alone τ_T or t_P. Third, while floats report salinity (or conductivity), temperature, and pressure triplets (or sometimes just the first two variables with an implicit pressure), they seldom (or never) telemeter a time stamp associated with each data scan. Thus, the exact ascent rate of the float is not well known, adding more uncertainty to the temperature time history.

3. The datasets

Two different datasets are used here to investigate CTD sensor response errors. The SBE-41CP errors are investigated using data from three deployments of ice-tethered profilers (ITP; Krishfield et al. 2006). The ITP comprises a profiling vehicle (with dimensions comparable to an Argo float) that uses a traction system to move up and down a ballasted wire-rope tether at about 0.27 m s^{-1}: about 3 times the typical ascent rate of an APEX float. Since the CTD is located at the top of the instrument with the intake duct pointing up, ascending profiles sample relatively undisturbed water in comparison to descending profiles.

A small surface buoy placed on the ice supports the tether. The buoy is equipped with an inductive modem (to communicate with the profiler via the wire rope) and an Iridium unit (to telemeter the acquired data back to shore).

The three prototype ITPs were equipped with SBE-41CPs, set up to acquire CTD data on both ascents and descents, and programmed to telemeter the full (24-bit resolution) 1-Hz CTD data. The first instrument deployed, ITP2, began making 6 one-way profiles per day between 10 and 750 dbar on 19 August 2004. Contact was lost on 29 September 2004 after it had reported 245 profiles; likely the ice supporting the surface buoy fractured. Two improved instruments (ITP1 and ITP3) were deployed on 16 and 24 August 2005, respectively, with instructions to occupy 4 one-way profiles per day between 10 and 760 dbar. These latter instruments are still reporting data as of this writing, but we limit our analyses to the first 659 and 627 profiles collected by ITP1 and ITP3, respectively, as of 27 January 2006.

The ITPs remained within a box bounded by 75.6°–79.3°N and 150.2°–133.2°W during the analysis period, a part of the Arctic Ocean called the Beaufort Sea, the deeper portions of which overlay the Canadian Basin. In this region the ITPs sampled a portion of the water column where cold, fresh Arctic halocline water overlays warmer, saltier Atlantic water. Between about 180 and 350 dbar ($-1.2 < \theta < 1.0$°C and $34.1 < S < 34.8$ PSS-78) the potential temperature–salinity (θ–S) relation is such that the Turner angle (Ruddick 1983) approaches values as low as -65°: conditions conducive to the diffusive form of double-diffusive instability. Susceptibility to double diffusion is corroborated by the presence of visible thermohaline staircases in the profiles (Fig. 2). The present analysis uses data from this portion of the water column obtained during uncontaminated ascending profiles. On occasion salinity spikes or abrupt shifts in the θ–S curve for a given profile suggest that the CTD might have been temporarily fouled. These profiles have been omitted from the present analysis. This first pass at quality control leaves 298, 119, and 305 profiles for ITP1, ITP2, and ITP3, respectively. Further outliers were discarded from individual response correction estimates as detailed below.

The SBE-41 errors are investigated using profiling float data. Between May 2001 and November 2005, the National Oceanic and Atmospheric Administration/Pacific Marine Environmental Research Laboratory (NOAA/PMEL) deployed 148 Webb Research Corporation APEX floats equipped with SBE-41 CTDs in the Pacific Ocean (see online at http://floats.pmel.noaa.gov). This array had reported a total of 5968 profiles as of 6 November 2005. The floats were programmed to drift at 1000 dbar (a few at 1500 dbar) for 10 days, and then either rise from that "park" pressure to the surface, or dive deeper to a "profile" pressure of 1200 or 2000 dbar before ascending. During their 3–6-h rise, the floats collected discrete samples of conductivity, temperature, and pressure at 60 to 73 preset pressure levels. The pressure interval between samples ranged from 4 to 8 dbar between the surface and 150 dbar, increasing to as much as 100 dbar between the deepest samples. After their ascent, the floats remained on the surface for about 10 h to telemeter their data via Service Argos before returning to the park pressure, completing a cycle. We also analyzed SBE-41 data from APEX floats
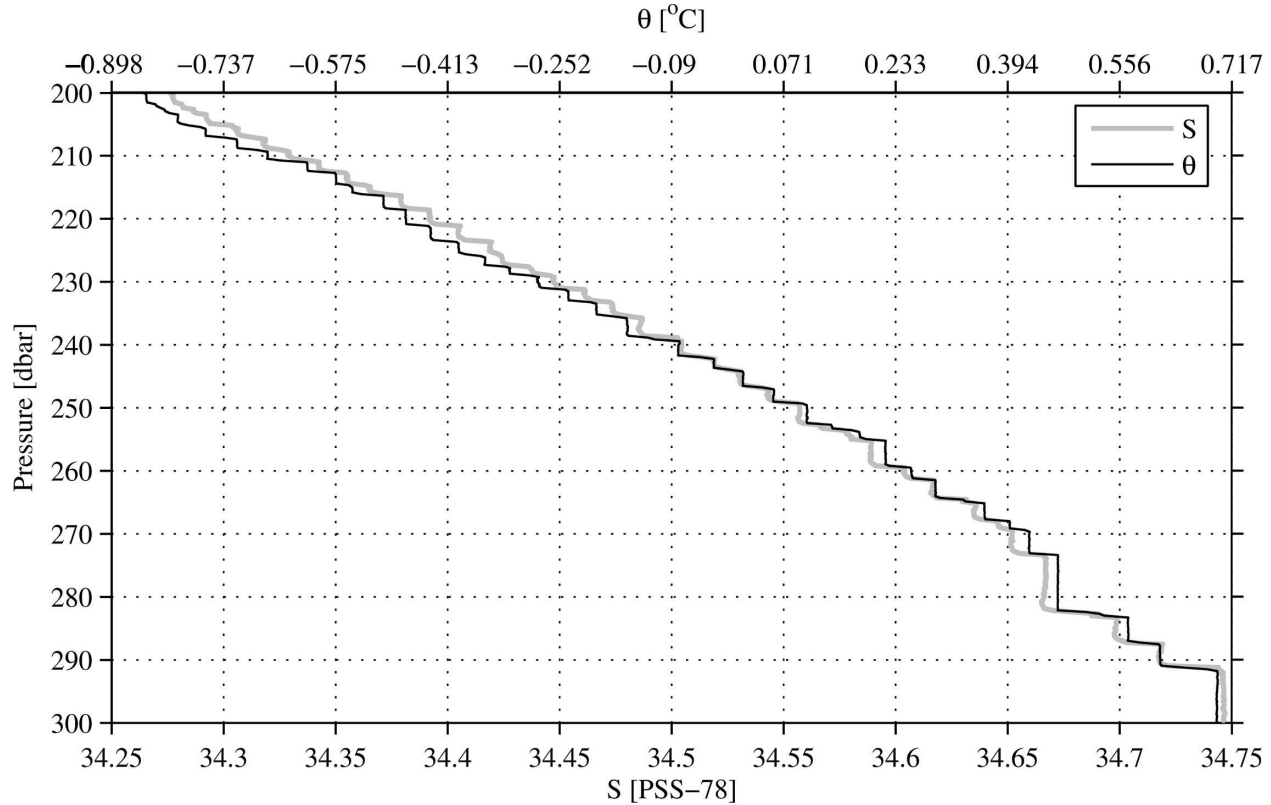
FIG. 2. A portion of potential temperature θ (°C), and salinity S (PSS-78), from ITP2, profile 31 (ascending), sampled 25 Aug 2004 at 77.0°N, 141.3°W plotted against pressure (dbar). Both variables have been response corrected as outlined in the text.

deployed under the direction of S. Riser at the University of Washington (UW). Since early 2000, his group has deployed about 375 such floats around the globe that returned at least 19 726 profiles as of 7 July 2005 (see online at http://flux.ocean.washington.edu/argo). Those floats were programmed similarly to the NOAA/PMEL floats, except that they generally sampled at 10-dbar pressure intervals between the surface and 400 dbar, and at 50-dbar intervals between 400 dbar and their deepest sample. As detailed below, subsets of 115 NOAA/PMEL and 342 UW float profiles were selected for analysis.

4. SBE-41CP sensor response corrections

Since the SBE-41CP data from the ITPs are reported at full 1-Hz resolution, it is possible to estimate and apply three different sensor response corrections. (The CTD averaging interval is too long compared with the short conductivity time scale τ_C to allow correction of this short-term cell response.) Below we address the temperature sensor response, the temporal misalignment between temperature and conductivity measurements, and the conductivity cell thermal mass error.

a. SBE-41CP thermistor response

The nominal time constant for the SBE-41CP thermistor ($\tau_T = 0.53$ s) is marginally shorter than both the instrument averaging time of 0.7 s and the sampling rate of 1 Hz. Therefore, given very sharp thermal staircases such as were sampled by the ITPs, the transient response of the sensor should be evident. Indeed, rather than sharp, symmetric temperature structure at the top and bottom of a given layer, the recorded temperature upon crossing the lower interface relaxes toward the layer value over one or more scans (Fig. 3). We correct for the finite response of the thermistor following Fofonoff et al. (1974) by using

$$T_o = T + \tau_T \frac{dT}{dt}, \tag{2}$$

where T_o is the true temperature and T is the measured temperature. To apply (2) we interpolate the data to a 10-Hz time series using a shape-preserving piecewise cubic interpolation, apply (2) to the result using first differences, then resample the corrected data to its original 1-Hz resolution. A search procedure was developed to determine the optimal τ_T for each profile
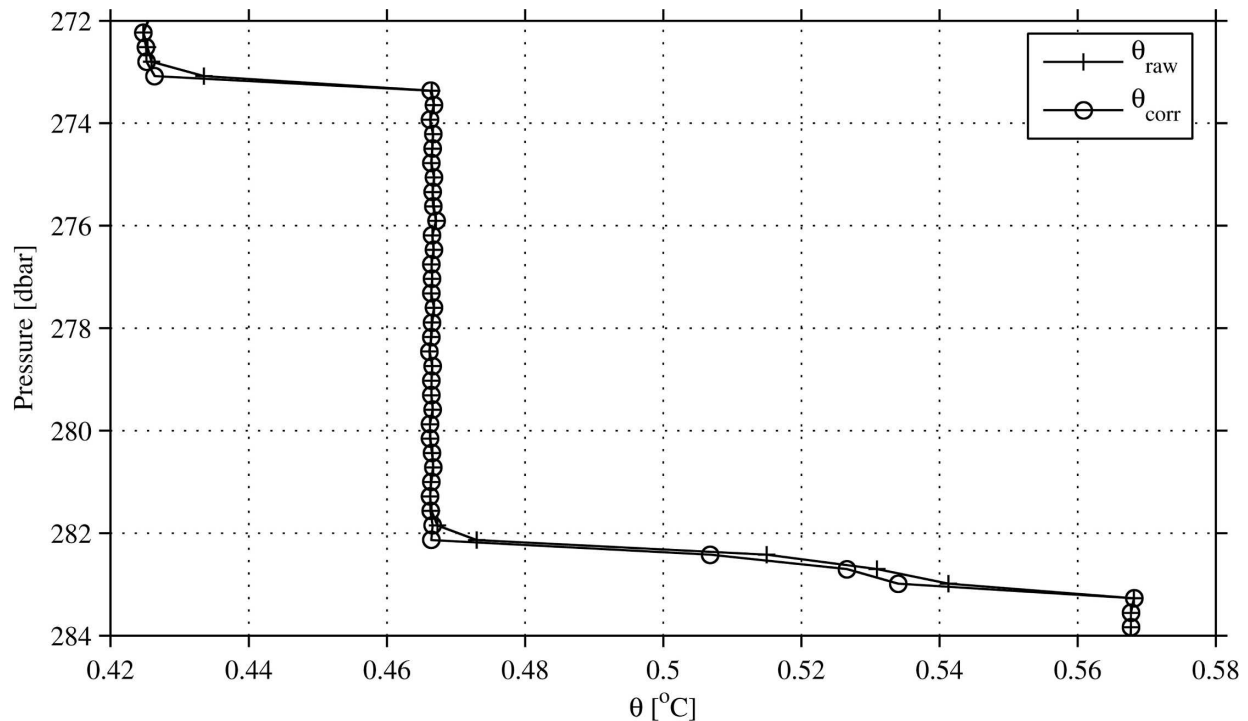
FIG. 3. Expanded view of the raw (solid line with pluses at data locations) and lag-corrected (solid line with circles at data locations) potential temperature profile, θ (°C) from a segment of ITP2, profile 31 (ascending).

under the assumption that the layers in the staircase were truly homogeneous. For the portion of each CTD time series exhibiting staircase stratification, the lag in (2) that maximized the number of points with the first differences in θ of magnitude $<0.5 \times 10^{-3}$°C was determined. The 0.5×10^{-3}°C noise threshold was selected by visual inspection. The minimization sharpens high-gradient regions and lengthens homogeneous regions.

All three instruments have long runs of ascending profiles with optimal $\tau_T \sim 0.4$ s, including all of the profiles from ITP2. However, ITP1 profiles 123–255 and 309–323 have values closer to 1 s or more, as do ITP3 profiles 47–469. These profiles with higher than expected lag values may indicate some subtle, intermittent problem that increases the apparent thermistor time lag without affecting the large-scale θ–S relation in an obvious manner. These profiles were excluded from subsequent analysis. The two long runs of odd profiles began in late summer, when organisms that might get lodged in a CTD duct were likely most prevalent. For the 242, 118, and 99 ascending profiles from ITP1, ITP2, and ITP3 we retained, the median $\tau_T = 0.39$, 0.37, and 0.40 s, respectively. The corresponding interquartile ranges are 0.13, 0.17, and 0.09 s. These statistics are quoted rather than means and standard deviations be-

cause a few outliers remain even after the suspect profiles were discarded, and some of the lag distributions appear skew (Fig. 4).

The thermistor response correction tends to make vertical temperature gradients thinner and sharper and the vertically homogeneous regions thicker (Fig. 3) as expected. In addition, the temperature correction helps ameliorate spikes in raw salinity data such as those about the high gradient regions near 273 and 283 dbar surrounding an ~8-m-thick homogeneous layer in ITP2 profile 31 (Fig. 5).

b. SBE-41CP sensor physical separation correction

Correction for the physical separation of temperature and conductivity sensors can also help to minimize salinity spikes within thermohaline staircases (Lueck and Picklo 1990). To determine this correction, t_P, for each of the selected profiles, the following steps were taken with the staircase segment time series. Pressures were filtered with a 15-point Hanning filter to reduce digitization noise and the temperature data were corrected for finite thermistor response as described above. Then, beginning with an initial guess at t_P, a search procedure was again performed. The conductivity was time shifted by t_P using a shape-preserving
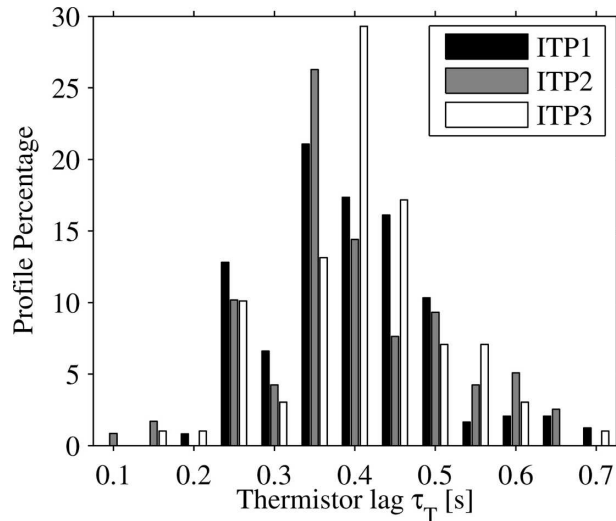
FIG. 4. Histograms (in 0.05-s bins) of the optimal thermistor lag τ_T (s) estimates derived for the selected ITP profiles from the three instruments that were analyzed.

piecewise cubic interpolation. The S and θ were calculated and a linear fit was made to the θ–S relation there. Then the standard deviation of the first differences of the actual S and those predicted from the first differences of θ and the slope of the linear fit was calculated. The conductivity time shift that minimized this standard deviation was found for each profile.

Interestingly, the derived conductivity time shifts (Fig. 6) are smaller than the 0.20-s estimate from the SBE empirical formula. For the 244, 119, and 100 retained profiles, the medians are $t_P = +0.08$ s, $+0.02$ s, and -0.01 s for ITP1, ITP2, and ITP3, respectively, with corresponding interquartile ranges of 0.05, 0.07, and 0.08 s. Given these relatively small numbers compared with the 1-Hz sample rate and the size of the spread in the estimates, it is not clear that application of time shifts is truly warranted. For ITP2, the salinity profiles with (Fig. 5) and without (not shown) a time shift applied are very similar even in high gradient regions. Simply correcting for the finite response of the thermistor turns out to eliminate most of the small-scale salinity spiking.

c. SBE-41CP conductivity cell thermal mass correction

With the thermistor response corrected using the median τ_T derived for each instrument, and (although small) the median time shifts, t_P, for each instrument applied, we turn to the conductivity cell thermal mass error. The selected portions of each profile exhibiting thermohaline staircase stratification are ideal for this task (Lueck and Picklo 1990). The cell thermal mass effect is clearly visible in the data segment examined previously (Fig. 5). Here the ITP rises through a 0.5°C temperature step in about 5 s between ~283 and 282 dbar. After passage through this gradient, θ remains constant from about 282 to 274 dbar, but salinity derived without a thermal mass correction applied to the temperature data exhibits an exponential relaxation to constant S by 276 dbar until the next gradient region is reached near 273 dbar. The salinity profile estimated with correction applied as detailed below is nearly uniform with depth where θ is uniform, as one would expect in a thermohaline staircase.

By eye, the exponential decay time scale for the conductivity cell thermal mass error τ_{CTM} seems to be about 7 s (i.e., 7 data points for these 1-Hz samples). The seawater equation of state is such that a temperature error of 0.001°C results in a salinity error of roughly 0.001 PPS-78 if left uncorrected. Based on the response model in (2), after passing through a constant temperature gradient region (of magnitude dT/dt) for a few decay times, the conductivity cell thermal mass error should result in a temperature anomaly in the conductivity cell that approaches the value $\alpha(dT/dt)\tau_{CTM}$. Subject to the caveat that the ITP takes less than one decay time scale to pass through the temperature gradient in this instance, one could hazard a guess at a lower bound on α with this information. For $\tau_{CTM} \sim 7$ s, $dT/dt \sim 0.025°C$ s^{-1}, and an initial error of 0.01 in salinity, we expect $\alpha > 0.06$. The actual value of α should be significantly higher, since the temperature gradient here is only a few seconds in duration.

We quantified the cell response parameters α and τ_{CTM} for each selected profile through a nonlinear minimization procedure. First, all runs were identified within each profile segment used previously of at least 20 data points (about 5 dbar) where consecutive first differences of θ varied by less than $1.5 \times 10^{-3}°C$ and θ varied over each run by less than $3.0 \times 10^{-3}°C$. Then a search for optimal α and τ_{CTM} was conducted that minimized the response-corrected salinity variance over these nearly constant temperature runs. In addition to the previous selection criteria, we discarded a few additional profiles for which estimates of $\alpha \times \tau_{CTM} > 2.0$ s. Interestingly, the profiles were discarded because the thermistor time scale τ_T, which was also large, had anomalously large values of τ_{CTM}, but anomalously small values of α, again suggesting some subtle problem with the instrument, perhaps related to flow rate. While in the example shown (Fig. 5), the fully corrected salinity profile appears to be slightly unstable, statistically the algorithm used yields uniform salinities in thermally homogeneous regions.
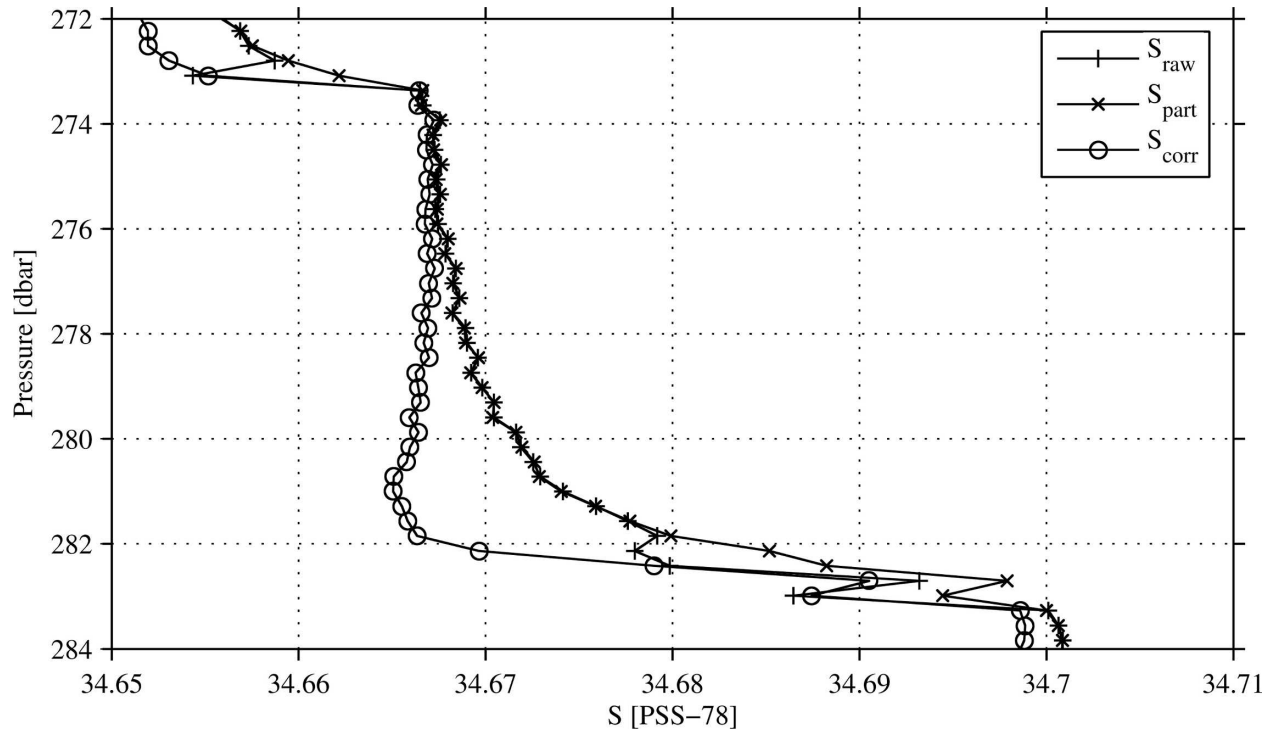
FIG. 5. Expanded view of salinity derived with the raw temperature and conductivity time series (plus symbols at each data point connected by a line), salinity partly corrected using time-shifted conductivity and lag-corrected temperature data (Xs with a line), and fully corrected salinity estimated with the previous corrections with temperature adjusted for conductivity cell thermal lag (circles with a line), from a small portion of ITP2 profile 31 (ascending) plotted against pressure (dbar). The time shift correction effects are insignificant compared to these others, so it is not shown separately. See Fig. 3 for the corresponding potential temperature profile.

Results for the analyzed profiles show some scatter (Fig. 7) with τ_{CTM} estimates ranging from 3 to 12 s, and α values from 0.08 to 0.25. While individual points for each instrument do not lie exactly on a curve defined by
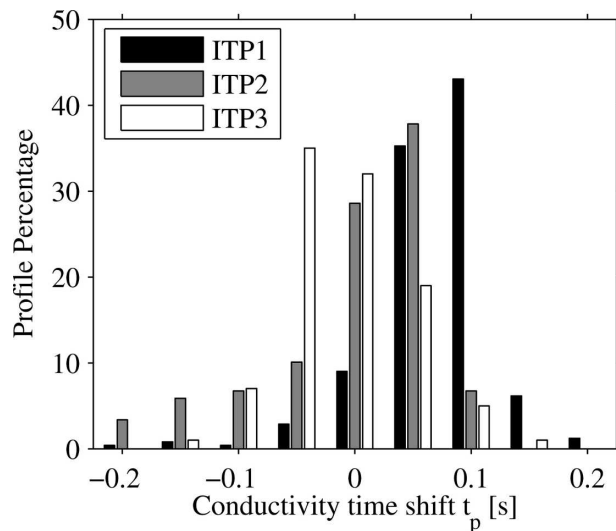

FIG. 6. Histograms of conductivity time shift t_P (s) estimates from the analyses of individual profiles from ITP1, ITP2, and ITP3 in 0.05-s bins.

constant $\alpha \times \tau_{CTM}$, neither do they scatter along a straight line. If they scattered around a straight line, the best estimates of α and τ_{CTM} would likely be their mean values. However, since they scatter along a curve, median values for each model parameter are probably more likely to lie along that curve.

For the 207, 95, and 89 retained profiles, the medians for τ_{CTM} are 6.15, 7.21, and 7.83 s for ITP1, ITP2, and ITP3, respectively (Fig. 7). Their corresponding interquartile ranges are 1.68, 2.96, and 3.02 s. The medians for α are 0.147, 0.165, and 0.120 for ITP1, ITP2, and ITP3, respectively, with corresponding interquartile ranges of 0.032, 0.038, and 0.031. The products of median α and τ_{CTM} values for these instruments are 0.90, 1.19, and 0.94 s, respectively. Using the appropriate median values for each ITP, salinity calculated from the response-corrected conductivity and temperature data looks much more like the corrected temperature profile (e.g., Fig. 5).

d. SBE-41CP sensor corrections viewed in the frequency domain

Spectral analysis assesses relative responses of temperature (T) and conductivity (C) versus frequency.
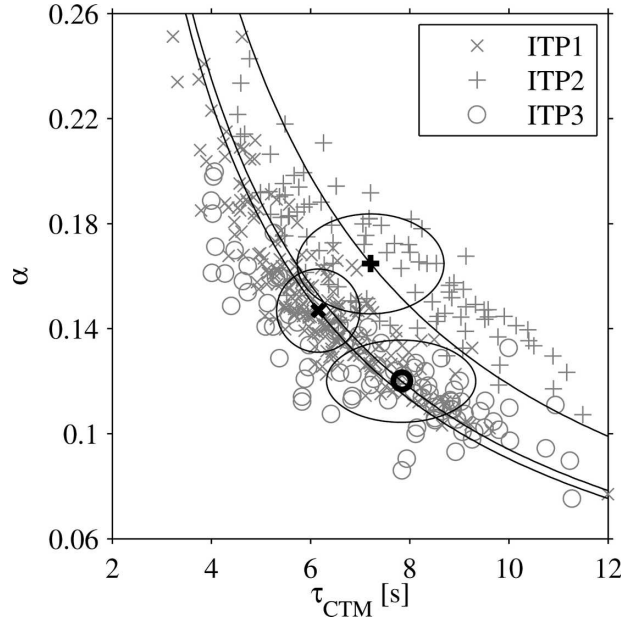
FIG. 7. Values of conductivity cell thermal mass correction model parameters α and τ_{CTM} for each profile analyzed from ITP1 (gray Xs), ITP2 (gray plus signs), and ITP3 (gray circles). Medians (black symbols) and interquartile ranges (gray ellipses) are plotted for all three instruments. Curves for constant median values of $\alpha \times \tau_{CTM}$ (thin black lines) are also shown.
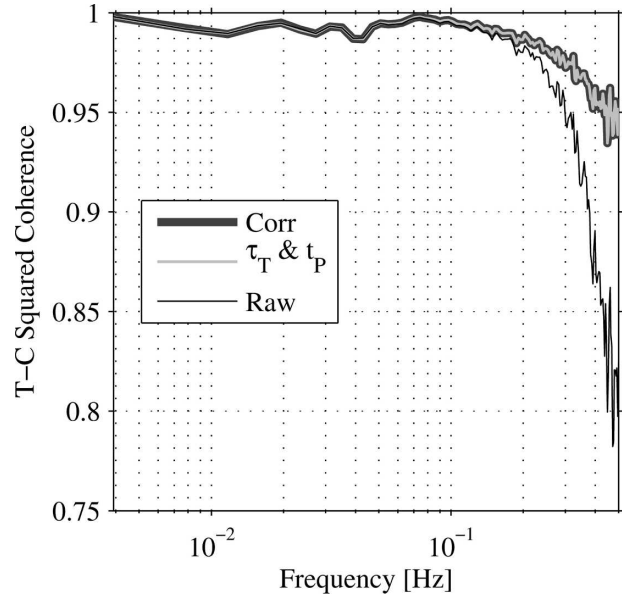

FIG. 8. Mean squared coherence between temperature (T) and conductivity (C) from the analysis of 256-point data segments centered on 240 dbar from 118 selected ascending profiles reported by ITP2. Raw (thin black line), thermistor-response corrected and conductivity shifted (medium thickness light gray line), and fully sensor response-corrected, including conductivity cell thermal mass, data (thick dark gray line) are displayed. Conductivity time-shift correction effects are insignificant compared to those of the other corrections, so it is not shown separately

We analyze 256-point segments of T and C data from 118 clean ascending ITP2 profiles. The data segments are centered on 240 dbar and lie chiefly between 205 and 275 dbar. These segments are used because they have a tight and nearly linear T–C relation. Prior to spectral analysis we remove linear fits from both the temperature and conductivity data segments, then apply a Hanning window to reduce edge effects. The mean of the square of the slopes of the T fit divided by the C fit is 0.79, representative of the dominant T/C energy ratio found at the lowest frequencies (longest vertical wavelengths). Since we are looking mostly at energy ratios, squared coherences, and phase relations between T and C, results are fairly insensitive to these preprocessing details.

The mean squared coherence for the T–C spectra of the raw data (Fig. 8) is quite high, about 0.99 at low frequencies, but starts to tail off to lower values at frequencies above about 0.1 Hz, nearly reaching 0.8 at the Nyquist frequency. The T/C energy ratio for the raw data has a similar pattern (Fig. 9). Interestingly, this ratio is about 1 (despite the dominant 0.79 value derived from the linear fits) from the lowest frequencies up to about 0.1 Hz, and then falls off to about 0.4 by the Nyquist frequency. The T–C phase for the raw data (Fig. 10) is slightly negative for frequencies below 0.05

Hz, but is strongly positive for higher frequencies, peaking at a value above 0.3 radians at about 0.3 Hz.

After application of the thermistor response correction and the conductivity time shift described in sections 4a and 4b, the mean squared T–C coherence is much improved at high frequency, being nowhere less than 0.95 (Fig. 8). The very small time shift of the conductivity data makes a negligible difference in all these plots compared with the very noticeable effects of the thermistor response correction, so the effects of these two corrections are shown together. Similarly, the T/C energy ratio for these partly corrected data is near unity throughout at all frequencies (Fig. 9). In phase space (Fig. 10), the large peak at high frequencies seen with the raw data is nearly eliminated by these corrections, as expected, with only small positive phases remaining for frequencies above 0.25 Hz. But larger negative phases are obtained at lower frequency, where the conductivity cell thermal mass error is most noticeable.

Application of the conductivity cell thermal mass correction to the temperature data, as described in section 4c, results in a temperature record that best matches the conductivity record in frequency space. The mean squared T–C coherence of the fully corrected data (Fig. 8) does not change much from the previous
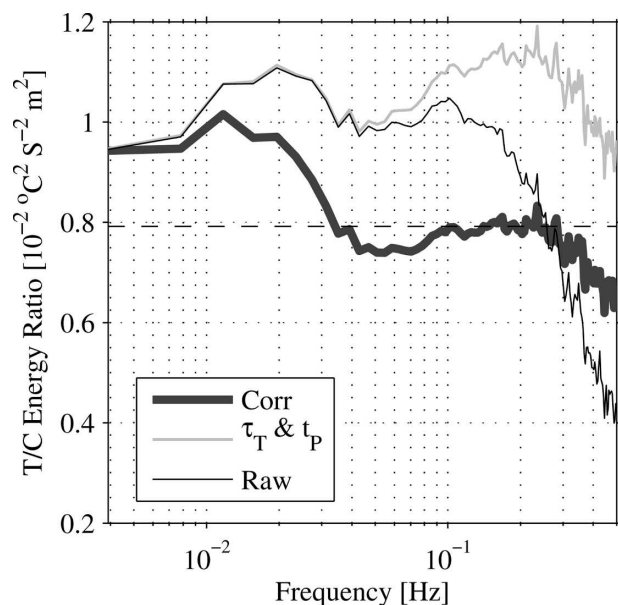
FIG. 9. Mean T/C spectral energy ratio for raw (thin black line), thermistor lag-corrected and conductivity time-shifted (medium thickness light gray line), and fully corrected (thick dark gray line) data from ITP2. The large-scale energy ratio (dashed line) is computed from the mean squared ratios of slopes of linear fits to the $T–C$ data. Other details are the same as in Fig. 8.

FIG. 10. Mean $T–C$ spectral phase for raw (thin black line), thermistor-response-corrected and conductivity time shifted (medium thickness light gray line), and fully corrected (thick dark gray line) data from ITP2. The zero phase (horizontal dashed line) is the target. Other details are the same as in Fig. 8.

corrections. However, the T/C energy ratio for the fully corrected data (Fig. 9) is close to the dominant large-scale value of 0.79 (as determined from the squares of the ratios of the slopes of the linear fits removed from the data) for frequencies higher than 0.03 Hz (vertical wavelengths shorter than about 9 dbar). Curiously, the ratio stays near unity for lower frequencies (longer wavelengths). The elevation likely results from ocean dynamics, perhaps lateral processes. The positive effects of the full suite of sensor corrections are very clear in the $T–C$ phase relation (Fig. 10), with phases uniformly near zero except for a small region around 0.35 Hz where the phase approaches 0.05 rad.

5. Conductivity cell thermal mass error in the SBE-41

An artifact likely resulting from the conductivity cell thermal mass error is apparent in many Argo float profiles that exhibit a well-defined (in temperature) surface mixed layer that caps a region with large vertical temperature gradient (Fig. 11). If, as is frequently the case, the observed temperature decreases with depth in the upper ocean, the deepest reported data point (and sometimes the deepest two values) in the thermally mixed surface layer will sometimes be anomalously fresh relative to the points above. These low-salinity
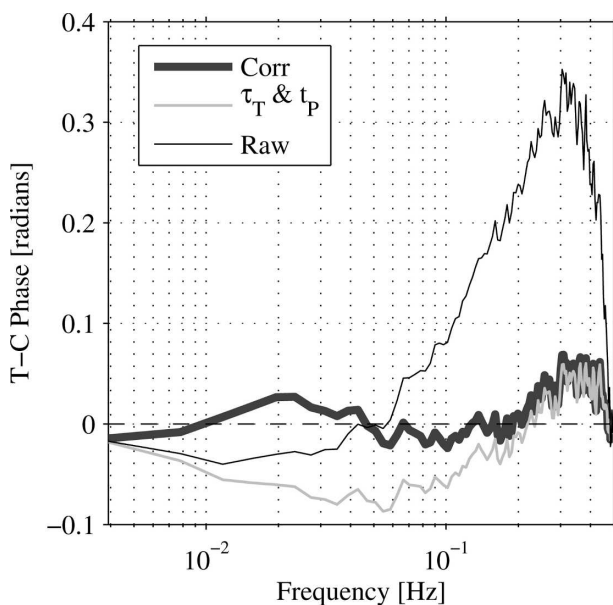
values are statically unstable and thus are likely artifacts of sensor response errors. However, the intermittent pumping strategy and coarse sampling interval of float-mounted SBE-41 CTDs make detecting, modeling, and correcting cell thermal mass errors problematic, and estimating and correcting any short time-scale mismatch between the temperature and conductivity sensor responses impossible.

We quantified the conductivity cell thermal mass error correction coefficients for SBE-41 float data by focusing on profiles with a well-defined thermal mixed layer above a region with significant vertical temperature gradient. Adopting a constant ascent rate of 0.09 dbar s^{-1} to translate pressure differences between points to time differences, we selected profiles in which the surface mixed layer contained at least three reported sample levels in which θ was within 0.01°C of the shallowest reported value and $|d\theta/dt| > 0.01$°C s^{-1} just below the mixed layer. Through successive application of the cell thermal mass correction to the selected profiles, we searched for values of α and τ_{CTM} that minimized the absolute value of the difference between the mean response-corrected potential density of the bottom two points of the thermally mixed layer and the mean uncorrected potential density in the rest of the mixed layer. Because the correction procedure is in the form of a discrete time step filter, it was necessary to interpolate the temperature and salinity time series to a
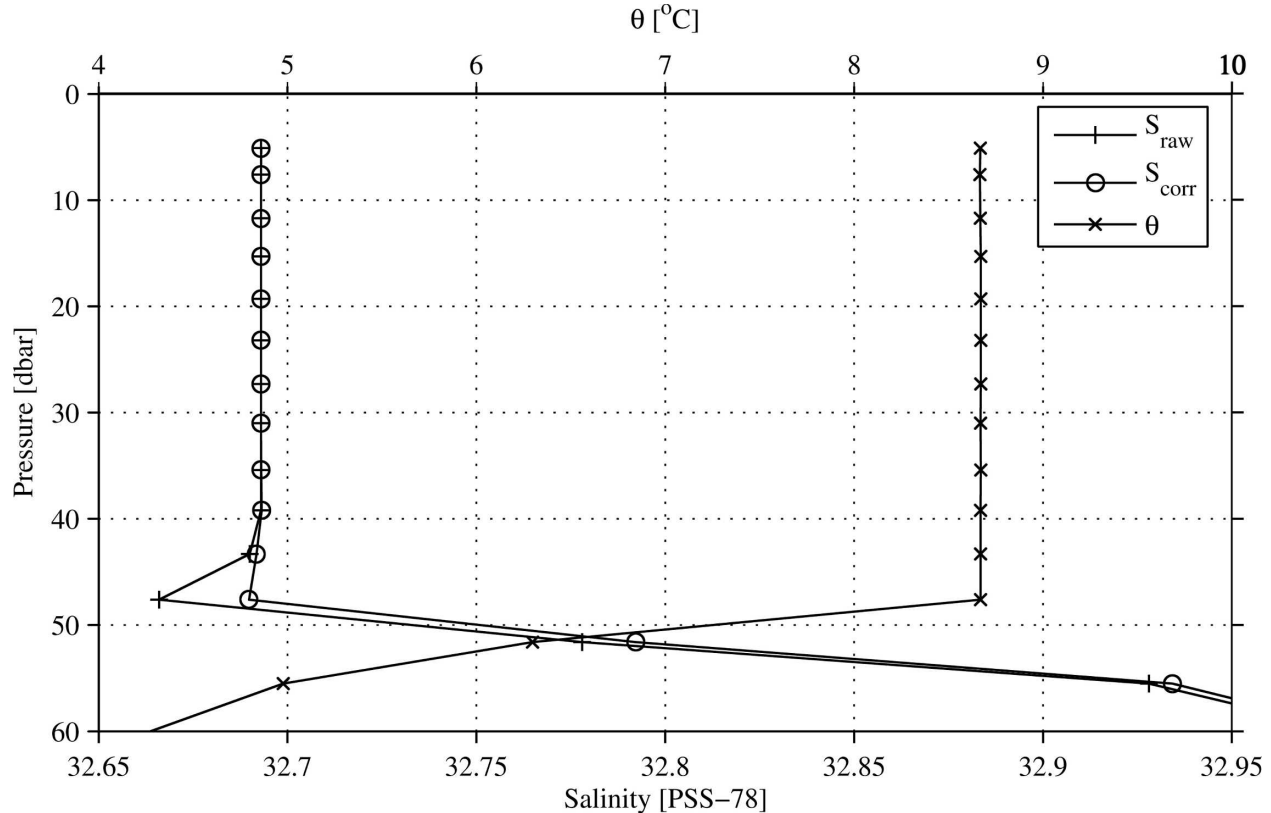
FIG. 11. Raw salinity (plus signs at each data point connected by a line), corrected salinity (circles with a line) and potential temperature, θ (Xs with a line), (°C) from profile 13 of Argo float World Meteorological Organization (WMO) ID 490017. The float is a Webb Research Corporation APEX260 equipped with a Sea-Bird Electronics SBE-41 CTD. The profile was collected on 12 Oct 2002 at 52.45°N, 160.27°W. The corrected salinity was derived using median conductivity cell thermal mass correction model coefficients $\alpha = 0.0267$ and $\tau = 18.6$ s.

regular time grid (we chose 1 Hz for our calculations) before estimating model coefficients and applying these corrections to the data. Once the corrections were applied to the 1-Hz dataset, the corrected dataset was reinterpolated back to the original resolution. The optimal correction adjusts salinity so that the mixed layer profile is close to being statically stable (Fig. 11).

After discarding profiles for which our scheme returned improbable model coefficients, 115 and 342 profiles were selected from the floats deployed by NOAA/PMEL and by UW, respectively (Fig. 12). The median value of τ_{CTM} for the NOAA/PMEL floats is 20 s, with an interquartile spread of 24 s, and that of the UW floats is 16 s, with an interquartile spread of 32 s. The median value of α for the NOAA/PMEL floats is 0.023, with an interquartile spread of 0.019, and that for the UW floats is 0.028, with an interquartile spread of 0.011. These SBE-41 model parameters have a larger spread than those derived for the SBE-41CP datasets. This difference in spread reflects greater uncertainty in the values deduced for the SBE-41 sensors due to its

very infrequent sampling. Interestingly, the product of the median α and τ_{CTM} for the two groups of SBE-41 profiles were very similar: 0.46 and 0.45 s.

Two notable features of the individual thermal mass coefficient estimates for the UW floats are a clustering of αs around 0.025 for τ_{CTM} values between 0 and 20 s, and a cluster of τ_{CTM} values around 20 s from $\alpha = 0.025$ to higher values. These are manifestations of the minimization routine that was seeded with $\alpha = 0.02$ and $\tau_{CTM} = 25$ s. For profiles with only one anomalous data point in the mixed layer, the estimation of two model coefficients becomes an underdetermined problem. The minimization in these instances tends to either increase α or decrease τ_{CTM} while leaving the other variable virtually unchanged.

6. Discussion

Operationally, there remains the issue of repeatability for the sensor response coefficients for the SBE-41CP and SBE-41 CTDs (Table 1). For the three SBE-
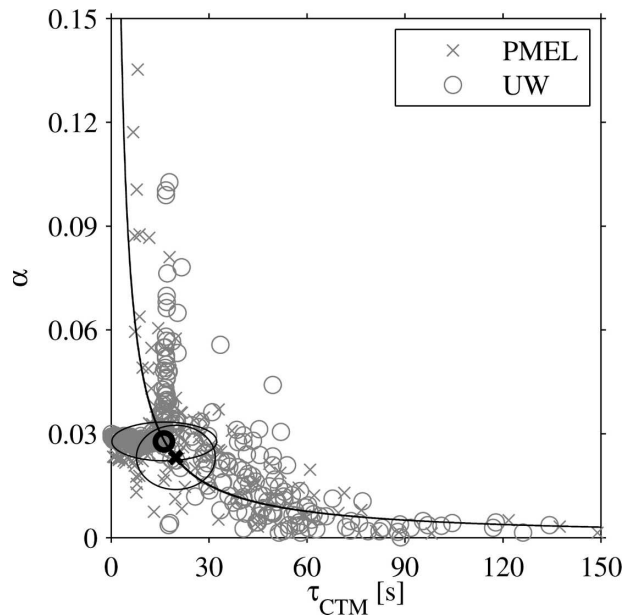
FIG. 12. Values of conductivity cell thermal mass correction model parameters α and τ_{CTM} for selected profiles from floats deployed by NOAA/PMEL (Xs) and by the University of Washington (circles). In all instances data are from SBE-41 CTDs mounted on APEX floats. Medians (black symbols) and the interquartile ranges (gray ellipses) are plotted for both sets of floats. Curves for constant median values of $\alpha \times \tau_{CTM}$ (thin black lines) are also displayed.

41CP CTDs analyzed, the weighted interquartile spread of thermistor lag τ_T is about a sixth and the total spread of median lags (0.03 s) only about a tenth of the weighted median, indicating that the thermistor time constant is well determined and reasonably consistent. The weighted interquartile spread of median time shift for conductivity relative to temperature t_P is about the same size as the weighted median, and the total spread of the medians time shifts (0.09 s) is even larger. These results suggest that if the thermistor lag has been corrected, a time shift of conductivity may not be warranted. The weighted interquartile spread of the conductivity thermal mass time scale τ_{CTM} is about a fifth and the total spread of median values (1.68 s) about a

TABLE 1. Weighted median values and interquartile spreads of sensor response corrections for SBE-41CP and SBE-41 CTDs.

| | SBE-41CP CTD | | SBE-41 CTD | |
	Median	Interquartile spread	Median	Interquartile spread
τ_T (s)	0.39	0.07	N/A	N/A
t_P (s)	0.05	0.04	N/A	N/A
τ_{CTM} (s)	6.68	1.31	18.6	19
α	0.141	0.019	0.0267	0.010

fourth of the median value, suggesting that it is fairly well determined. The weighted interquartile spread and the total spread of median amplitudes (0.045) for the correction amplitude α are again about a seventh and a fourth of the median value, suggesting that it is fairly well determined.

For the SBE-41 data analyzed, the sampling is too coarse to allow thermistor response correction or a time shift of conductivity relative to temperature. The weighted interquartile spread of the conductivity thermal mass time scale τ_{CTM} is similar to the median value (Table 1). The weighted interquartile spread of the correction amplitude α is about a third of the weighted median value. The large spreads for the SBE-41 correction parameters most likely result from the effects of coarse temporal (hence vertical) sampling on estimating these parameters for a given profile. Below, it is argued that application of the correction using coefficient median values makes statistical sense, even though individual profiles may not be perfectly corrected.

The conductivity thermal mass effect amounts roughly to a 0.01 PSS-78 error in data from a SBE-41CP transiting a $0.01°C \ s^{-1}$ temperature gradient. The error would be about 0.005 PSS-78 for an SBE-41 transiting the same temperature gradient. Floats ascending at 0.09 dbar s^{-1} through strong thermoclines can experience temperature gradients as large as $0.1°C \ s^{-1}$, although such gradients are rare. Thus, conductivity cell thermal mass errors for SBE-41CP-equipped floats could occasionally approach 0.1 PSS-78, and those for SBE-41-equipped floats might experience errors half that magnitude. Both these potential errors are well outside the Argo salinity accuracy target of 0.01. While large gradients are rare, approximately half of the PMEL profiles analyzed here sampled a temperature gradient of $0.02°C \ s^{-1}$ or more, a gradient sufficiently strong that the thermal mass error approaches the Argo salinity accuracy specification in the thermocline even for an SBE-41-equipped float. Given the typical ocean temperature stratification of warm water overlying cold, uncorrected data will tend to be biased fresh within and just above the thermocline.

The SBE-41 temporal resolution is coarse and irregular, and 1-Hz data are rarely reported from SBE-41CP CTDs on Argo floats. Sample times are rarely (if ever) reported. These practices complicate the correction of conductivity thermal mass errors in several ways. First, the relationship between pressure and time must be estimated to transform the reported vertical temperature gradient into a temporal gradient. For the APEX floats analyzed here, a constant rise rate of 0.09 dbar s^{-1} was assumed, even though the standard deviation of

available rise rate estimates is ± 0.03 dbar s^{-1}. This uncertainty introduces errors into the reconstructed temperature time history. In addition, the sparse vertical sampling (or resolution of reported data), only reaching as fine as 4–10 dbar in the upper ocean (corresponding to time intervals of 44–110 s), means that the time history of temperature is grossly underreported with respect to either model CTD's conductivity cell thermal mass error time scale (roughly 7 s for the SBE-41CP, and 19 s for the SBE-41). This coarse sampling introduces more uncertainty into the correction by aliasing temperature variations on shorter time scales than the sampling (or averaging, or subsampling) interval into the gradient estimates. Because of these uncertainties, we believe that a realistic confidence limit on the estimated corrections is about the magnitude of the corrections themselves. That is, we can remove bias in the reported salinity owing to the conductivity cell thermal mass error, but a conservative assessment of the uncertainty in the corrected salinity for any individual data point is thought to be about the magnitude of the correction itself.

Even if the correction is uncertain from point to point, an overall statistical salinity bias will still remain for uncorrected profiles, especially in and above the thermocline, owing to the large-scale vertical temperature gradient there. Hence, it makes sense to apply the correction to remove this bias in a statistical sense even if the available profile data are not optimum for the correction. To apply the correction following conventional methods (Lueck and Picklo 1990; Morison et al. 1994) it is best to first convert the temperature data from a function of pressure to one of time using the best available estimate of float ascent rate, to interpolate the data to a uniform (e.g., 1 Hz) time series, to apply the corrections, and then to decimate back to the original resolution.

Often SBE-41 CTD equipped floats are programmed to sample at finer pressure intervals near the surface than at depth. Given the different heat exchange characteristics for the SBE-41 when the pump is on versus when it is off, the conductivity cell thermal mass error for the SBE-41 might be sensitive to the sample schedule. Here the SBE-41 correction coefficients were determined using upper-ocean data from one dataset having 4–8-dbar resolution (NOAA/PMEL) and another with 10-dbar intervals (UW). It is reassuring that resulting coefficients from our analyses are in rough agreement. Application of the method to other float datasets in which SBE-41 CTDs were programmed to sample at significantly different intervals might reveal how the error model coefficients vary with varying sampling intervals.

We note that the SBE-41CP data used to estimate the conductivity cell thermal inertia correction coefficients for that instrument were from ITPs that rise at about 0.27 dbar s^{-1}, a rate about 3 times that of profiling CTD floats. Our analysis of the ITP data may tend to underestimate the SBE-41CP correction coefficients for float applications for two reasons. First, although the CTD conductivity cells are encased in a polyurethane jacket that is relatively insulating compared with the glass itself, some heat is still exchanged between the conductivity cell and the external water. This exchange will increase as the flow past the exterior of the cell increases (Lueck 1990). In addition, because the duct intakes of SBE-41 and SBE-41CP CTDs face up while the exhaust ports are oriented perpendicular to the intakes, there is a pressure differential between intake and exhaust that varies with ascent rate. At a 0.09 dbar s^{-1} ascent speed, the pressure-induced flow velocity in the duct with the pump off may be about 0.008 m s^{-1}, but at triple the ascent speed, this flow velocity could be 9 times larger, or about 0.07 m s^{-1}. This value is more than a tenth of the estimated pumped flow of 0.64 m s^{-1} for the SBE-41CP. Thus, the ITP-mounted SBE-41CPs may have smaller conductivity cell thermal inertia errors than float-mounted SBE-41CPs. It would be instructive to deploy a profiling CTD float equipped with a SBE-41CP in a region of thermohaline staircases and telemeter back full-resolution data to check (and perhaps revise) the model coefficients estimated here.

A few modifications could be made to existing technology to reduce uncertainty in the conductivity cell thermal mass corrections. First, the float buoyancy engine software could be modified to produce a known, relatively uniform ascent rate, reducing the error in estimating the time history of temperature sampled by the floats. Alternately, the floats could report sample time in addition to temperature, salinity, and pressure. Second, reporting data at increased temporal (hence vertical) resolution would result in improved ability to reduce the uncertainty of the corrected salinities. Increased vertical resolution should be more easily realized with floats that communicate through Iridium. Third, SBE-41CP software could be modified to apply the sensor response corrections estimated here to the full-resolution 1-Hz data prior to bin averaging or subsampling the data. But before this step is taken, it would be prudent to estimate the SBE-41CP correction coefficients at typical float rise rates. To improve sensor response corrections, one might profile different models of CTDs through thermohaline staircases at a variety of ascent speeds and pump rates. It would also be desirable to determine how the correction coefficients vary with varying rise rates.

REFERENCES

Fofonoff, N. P., S. P. Hayes, and R. C. Millard Jr., 1974: W.H.O.I./ Brown CTD microprofiler: Methods of calibration and data handling. Woods Hole Oceanographic Institution Tech. Rep. WHOI-74-89, 64 pp.

Gregg, M. C., and W. C. Hess, 1985: Dynamic response calibration of Sea-Bird temperature and conductivity probes. *J. Atmos. Oceanic Technol.,* **2,** 304–313.

Krishfield, R., and Coauthors, 2006: Design and operation of automated Ice-Tethered Profilers for real-time seawater observations in the polar oceans. Woods Hole Oceanographic Institution Tech. Rep. WHOI-2006-NN, 30 pp.

Lueck, R. G., 1990: Thermal inertia of conductivity cells: Theory. *J. Atmos. Oceanic Technol.,* **7,** 741–755.

——, and J. L. Picklo, 1990: Thermal inertia of conductivity cells: Observations with a Sea-Bird cell. *J. Atmos. Oceanic Technol.,* **7,** 756–768.

Morison, J., R. Andersen, N. Larson, E. D'Asaro, and T. Boyd, 1994: The correction for thermal-lag effects in Sea-Bird CTD data. *J. Atmos. Oceanic Technol.,* **11,** 1151–1164.

Roemmich, D., S. Riser, R. Davis, and Y. Desaubies, 2004: Autonomous profiling floats: Workhorse for broadscale ocean observations. *J. Mar. Technol. Soc.,* **38,** 31–39.

Ruddick, B., 1983: A practical indicator of the stability of the water column to double-diffusive activity. *Deep-Sea Res.,* **30A,** 1105–1107.